

Latest results on diboson and multiboson production from the CMS experiment

Javier Cuevas on behalf of the CMS Collaboration*

Universidad de Oviedo

E-mail: Javier.Cuevas@cern.ch

Recent measurements of diboson production in proton-proton collisions at the LHC, performed by the CMS Collaboration, are summarized. Studies of ZZ production, WZ and WW production at $\sqrt{s} = 13$ TeV, $WV \rightarrow \ell\nu q\bar{q}$ ($V = W^\pm$ or Z , $\ell = e$ or μ) at $\sqrt{s} = 13$ TeV, and $Z\gamma\gamma$ and $W\gamma\gamma$ at $\sqrt{s} = 8$ TeV are reported. Inclusive and differential cross section measurements and limits on anomalous triple gauge couplings are reported, as well as a measurement of the $Z \rightarrow 4\ell$ branching fraction.

Sixth Annual Conference on Large Hadron Collider Physics (LHCP2018)

4-9 June 2018

Bologna, Italy

*Speaker.

1. Introduction

Measurements of diboson and multiboson production (VV, VVV, where V is Z, W^\pm , or γ) at the CERN LHC provide insights into the electroweak gauge structure of the standard model (SM). Extensions of the SM predict additional processes with multiple bosons in the final state, then, any observed deviation of multiboson cross sections from their SM predictions could be an early sign of physics beyond the SM. With a large dataset at the unprecedented center-of-mass energy of 13 TeV, the CMS experiment [1] studies these processes at this new energy in detail. In this report, measurements of ZZ [2], WZ [3], WW [4], $WV \rightarrow \ell\nu q\bar{q}$ ($V = W^\pm$ or Z, $\ell = e$ or μ) [5], and $Z\gamma\gamma$ and $W\gamma\gamma$ [6] production are summarized. Full analysis details and results can be found in the references provided.

2. ZZ production

ZZ production provides a probe of neutral gauge boson interactions in the SM, and its cross section is highly sensitive to higher-order quantum chromo-dynamics (QCD) corrections. The 4ℓ final state, where $\ell = e$ or μ , can be fully reconstructed and has small backgrounds. This final state is studied at a center-of-mass energy of 13 TeV with the CMS detector at the LHC and the data sample used corresponds to an integrated luminosity of 35.9 fb^{-1} . The ZZ production cross section is measured using events with two opposite-sign, same-flavor lepton pairs produced in the mass region $60 < m_{\ell+\ell^-} < 120 \text{ GeV}$. The major background contributions arise from Z boson and WZ diboson production in association with jets and from $t\bar{t}$ production. In all these cases, particles from jet fragmentation can satisfy both lepton identification and isolation criteria, and be misidentified as signal leptons. The probability for such objects to be selected is measured from a sample of $Z + \ell_{candidate}$ events. Triboson, $t\bar{t}Z$, and Higgs boson backgrounds are estimated with simulated samples. The four-lepton invariant mass distribution is shown in Fig. 1 (left), along with SM predictions with which it generally agrees. The ZZ production cross section is measured to be:

$$\sigma(\text{pp} \rightarrow \text{ZZ}) = 17.2 \pm 0.5 \text{ (stat.)} \pm 0.7 \text{ (syst.)} \pm 0.4 \text{ (theo.)} \pm 0.4 \text{ (lumi.) pb}$$

consistent with standard model predictions. The total ZZ cross section is shown in Fig. 1 (right) as a function of the proton-proton center-of-mass energy. Results from CMS and ATLAS are compared to predictions from MATRIX and MCFM with the NNPDF3.0 PDF sets and fixed scales $\mu_F = \mu_R = m_Z$. The MATRIX prediction uses PDFs calculated at NNLO, while the MCFM prediction uses NLO PDFs. The uncertainties are statistical (inner bars) and statistical and systematic added in quadrature (outer bars). The band around the MATRIX predictions reflects scale uncertainties, while the band around the MCFM predictions reflects both scale and PDF uncertainties. The Z boson branching fraction to four leptons is measured by comparing the measured $Z \rightarrow 4\ell$ fiducial cross section to the $Z \rightarrow 2\ell$ fiducial cross section, with a correction for nonresonant four-lepton production and is determined to be:

$$\mathcal{B}(Z \rightarrow 4\ell) = 4.83_{-0.22}^{+0.23} \text{ (stat.)} {}_{-0.29}^{+0.32} \text{ (syst.)} \pm 0.08 \text{ (theo.)} \pm 0.12 \text{ (lumi.)} \times 10^{-6}$$

for events with a four-lepton invariant mass in the range $80 < m_{4\ell} < 100 \text{ GeV}$ and a dilepton mass $m_{\ell\ell} > 4 \text{ GeV}$ for all opposite-sign, same-flavor lepton pairs. The results agree with standard

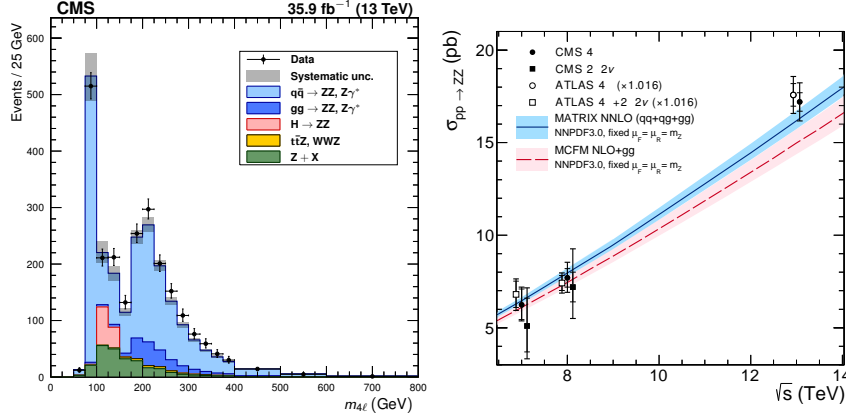


Figure 1: (left) Distribution of the four-lepton invariant mass $m_{4\ell}$ and of all Z/γ^* bosons in selected four-lepton events. Vertical bars on the data points show their statistical uncertainty. Shaded grey regions around the predicted yield represent combined statistical, systematic, theoretical, and integrated luminosity uncertainties. (right) The total ZZ cross section as a function of the proton-proton center-of-mass energy [2].

model predictions. The measurement of the differential cross sections provides detailed information about ZZ kinematic properties. The observed yields are unfolded using an iterative technique. The three decay channels, $4e$, 4μ , and $2e2\mu$, are combined after unfolding because no differences are expected in their kinematic distributions. The generator-level leptons used for the unfolding are dressed. Fig. 2 (left) shows the normalized differential four-lepton cross section as a function of $m_{4\ell}$. This includes contributions from the Z and Higgs boson resonances and continuum ZZ production. The presence of anomalous trilinear gauge couplings (aTGCs) would increase the yield of events at high four-lepton masses. Fig. 2 (right) presents the distribution of the four-lepton reconstructed mass of events with both Z bosons in the mass range 60–120 GeV for the combined $4e$, 4μ , and $2e2\mu$ channels. This distribution is used to set the limits on possible contributions from aTGCs. Two simulated samples with nonzero aTGCs are shown as examples, along with the SM distribution simulated by both SHERPA and POWHEG. The observed one-dimensional 95% CL limits for the $f_4^{Z,\gamma}$ and $f_5^{Z,\gamma}$ anomalous coupling parameters are:

$$-0.0012 < f_4^Z < 0.0010, \quad -0.0010 < f_5^Z < 0.0013$$

$$-0.0012 < f_4^\gamma < 0.0013, \quad -0.0012 < f_5^\gamma < 0.0013.$$

These are the most stringent limits to date on anomalous ZZZ and $ZZ\gamma$ trilinear gauge boson couplings, improving on the previous strictest results from CMS by factors of two or more.

3. WZ production

WZ production is sensitive to higher-order QCD corrections and the details of tri-linear gauge boson couplings. The final state provides a clean channel with manageable backgrounds. The signature of the process is three well-identified, isolated leptons in association with a large imbalance of transverse momentum of detected particles (the magnitude of which is called the missing energy, E_T^{miss}) associated to the undetected neutrino. To reduce contributions from $t\bar{t}$ events [3],

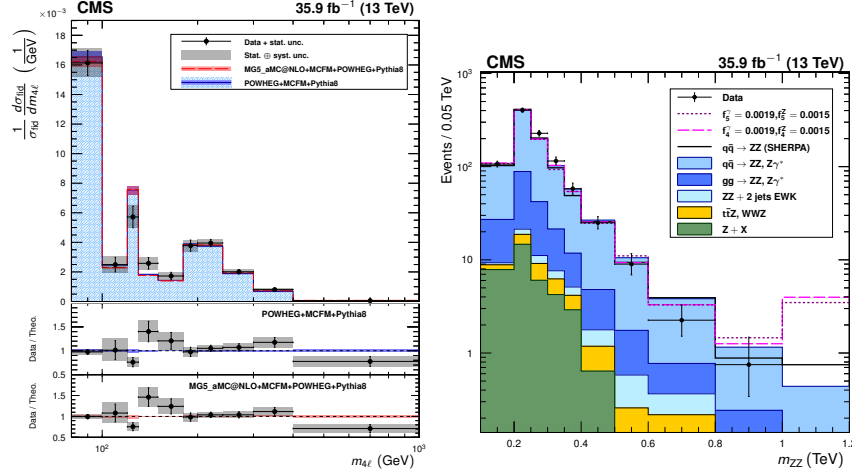


Figure 2: (left) The normalized differential four-lepton cross section as a function of the four-lepton mass. SM $gg \rightarrow H \rightarrow ZZ^*$ production is included, simulated with POWHEG. (right) Distribution of the four-lepton reconstructed mass for the combined $4e$, 4μ , and $2e2\mu$ channels. Unfilled histograms represent examples of aTGC signal prediction [2].

the two leptons constituting the Z boson candidate are required to have an invariant mass satisfying $76 < m_{\ell\ell} < 106$ GeV, and the trilepton invariant mass, $m_{3\ell}$, is required to be more than 100 GeV to exclude a region where production of Z bosons with final-state radiation is expected to contribute. The background contributions in this analysis are divided into two categories: background processes with prompt isolated leptons, e.g., ZZ , $Z\gamma$, $t\bar{t}Z$, and background processes from nonprompt leptons from hadrons decaying to leptons inside jets or jets misidentified as isolated leptons, primarily Z +jets and $t\bar{t}$. The background processes with prompt leptons are estimated from simulation. The processes with at least one nonprompt lepton are estimated from data. The nonprompt background contribution is evaluated using the “tight-to-loose” method. The method estimates the probability that a *loose* candidate is misidentified as a *tight* lepton and applies this probability to control regions with *loose* candidates to estimate the resulting contribution to the signal region. These *loose* candidates are selected with relaxed lepton identification and isolation requirements. The uncertainties in background contributions from both flavors of nonprompt leptons are determined by combining the uncertainties in the measured values of the misidentification probabilities and the statistical uncertainties due to the limited number of events in the control regions. The systematic uncertainty in the misidentification probability is 30% for both electrons and muons. The invariant mass distributions for all channels combined are shown in Fig. 3 and compared to the SM expectations and to the backgrounds estimated from data with the full WZ selection requirements. The fiducial $WZ \rightarrow \ell\nu\ell'\ell'$ cross section for $p_{\text{T}}^{\ell} > 20, 10$ GeV, $p_{\text{T}}^{\ell'} > 20$ GeV, all leptons within $|\eta| < 2.5$, $60 < m_{\ell\ell'} < 120$ GeV, and invariant mass of any same-flavor opposite-sign lepton pair above 4 GeV is

$$\sigma_{\text{fid}}(\text{pp} \rightarrow WZ \rightarrow \ell\nu\ell'\ell') = 258 \pm 21 \text{ (stat.)}_{-20}^{+19} \text{ (syst.)} \pm 8 \text{ (lumi.) fb},$$

corresponding to a total cross section for the range $60 < m_{\ell\ell'} < 120$ GeV of

$$\sigma(\text{pp} \rightarrow WZ) = 39.9 \pm 3.2 \text{ (stat.)}_{-3.1}^{+2.9} \text{ (syst.)} \pm 0.4 \pm 1.3 \text{ (lumi.) pb}.$$

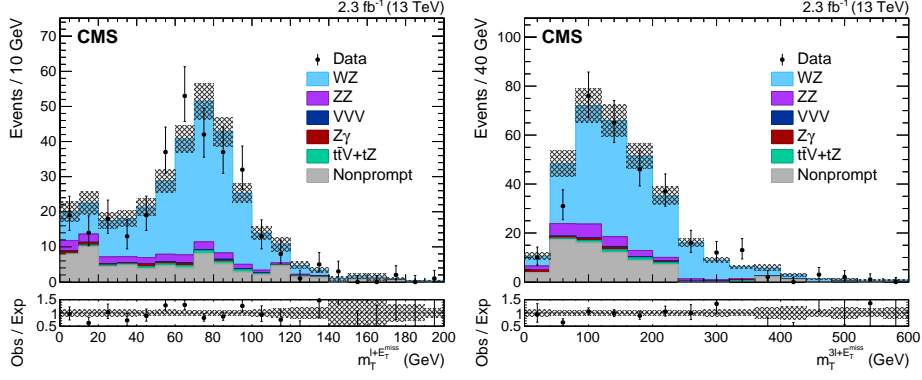


Figure 3: (left) The transverse mass of the lepton from the W boson and the E_T^{miss} system. (right) The transverse mass of the three leptons and the E_T^{miss} system. The background shapes are taken from simulation or data, as described in the text [3].

The measured cross sections can be compared to the theoretical values of 274_{-8}^{+11} (scale) ± 4 (PDF) fb for the fiducial cross section and $42.3_{-1.1}^{+1.4}$ (scale) ± 0.6 (PDF) pb for the total cross section calculated with MCFM at NLO with NNPDF3.0 PDFs, with dynamic renormalization and factorization scales set to $\mu_R = \mu_F = m_{WZ}$. The measured total cross section can also be compared to the theoretical value of $50.0_{-1.0}^{+1.1}$ (scale) pb, available at NNLO via MATRIX [7] with fixed QCD scales set to $\mu_R = \mu_F = \frac{1}{2}(m_Z + m_W)$ and NNPDF3.0 PDFs. The values from MCFM with this scale choice are 291_{-13}^{+16} (scale) ± 4 (PDF) fb for the fiducial and $44.9_{-1.8}^{+2.2}$ (scale) ± 0.7 (PDF) pb for the total cross sections.

4. WW production

The leptonic final state in the W^+W^- channel consists of two oppositely charged, high p_T , isolated leptons not compatible with a Z boson decay, large missing transverse energy from the neutrinos recoiling against the two leptons, and a small number of jets. Selected events [4] contain exactly one electron and one muon with opposite charge and $p_T^\ell > 20$ GeV, which greatly suppresses contributions from Drell-Yan processes. The E_T^{miss} in the events is required to be larger than 20 GeV. Only events with zero or one reconstructed jets with $p_T^j > 30$ GeV and $|\eta^j| < 4.7$ are used in the analysis, which suppresses contributions from top-quark mediated processes. The measurement is performed separately for events with zero and one reconstructed jets. The statistical analysis is based on a simultaneous profile likelihood fit of the two signal regions corresponding to the 0-jet and 1-jet categories and their associated control regions for top-quark mediated background processes. The combination of the 0-jet and 1-jet categories is the nominal result. The W^+W^- cross section is measured to be 115.3 ± 10.3 (stat. + syst.) ± 3.6 (lumi.) pb, consistent with the NNLO theoretical prediction, which is $\sigma^{\text{NNLO}}(\text{pp} \rightarrow W^+W^-) = 120.3 \pm 3.6$ pb [8].

5. WV production

Additional operators that would lead to anomalous WW γ or WWZ couplings are considered

in this analysis by studying events with one W boson decaying to an electron or muon and neutrino and one W or Z boson decaying hadronically [5]. As the effects of the aTGCs are most dramatic at high boson momenta, only “boosted” hadronic boson decays are considered, where the hadronization products of the two final state quarks geometrically overlap to form a single large-radius jet. The analysis is split into WW and WZ final states using the invariant mass of the jet created as the result of the hadronic decay of W or Z bosons. This can provide discrimination between some aTGC though the limited resolution causes significant cross-contamination between the channels. In order to reduce contributions from W+jets backgrounds, jet-substructure techniques are used. To have a good discrimination against jets from gluon and single-quark hadronization, N-subjettiness [9] is used. The ratio between 2-subjettiness and 1-subjettiness, $\tau_{21} = \tau_2/\tau_1$, is found to be a powerful discriminant between jets originating from hadronic V decays and from gluon and single-quark hadronization. The W+jets background is suppressed by requiring a pruned mass [10] of $65 \text{ GeV} < M_{\text{pruned}} < 105 \text{ GeV}$ and $\tau_{21} > 0.6$ for the signal region. The signal regions with $M_{\text{pruned}} < 85 \text{ GeV}$ (WW region) and $M_{\text{pruned}} > 85 \text{ GeV}$ (WZ region) are treated separately. The normalizations of the W+jets and $t\bar{t}$ backgrounds are extracted from the M_{pruned} distribution in the data using a template fit. Systematic uncertainties are evaluated for the $t\bar{t}$, single-top quark and diboson processes using simulated samples. Limits are set on aTGCs using the data in the signal region and background estimates as shown in Fig. 4. Limits are set at 95% confidence level (CL) using a simultaneous unbinned maximum likelihood fit of the M_{WV} distributions in the four signal regions. Systematic uncertainties are included as nuisance parameters and limits are derived from contours of the negative logarithmic likelihood as function of the aTGCs. The effective field theory (EFT) parametrization used here is assumed to be valid at the energies relevant for this experiment, i.e. that the actual scale associated with new particles is much larger than the scale Λ to which the experiment is sensitive. In addition to the EFT parametrization, the limits are also computed in terms of the parametrization commonly used at LEP [11]. The resulting limits are given in Tab. 1.

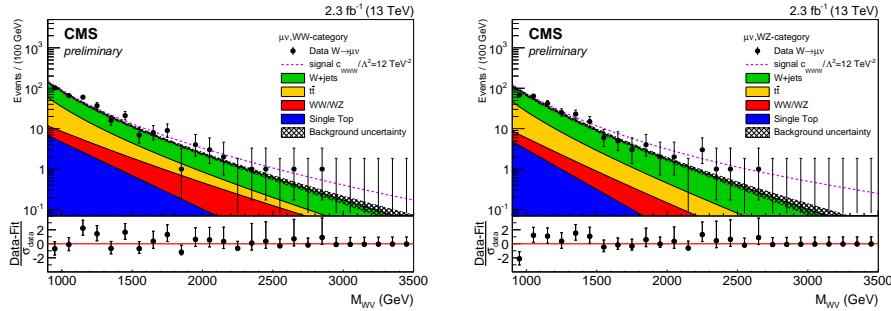


Figure 4: Comparison of the M_{WV} distribution in the data and background estimate for the muon channel, in the WW- and WZ-category. The pink line represents the sum of the backgrounds and a signal with an aTGC value of $c_{WWW} = 12 \text{ TeV}^{-2}$. Each figure also shows the difference between data and the SM prediction, divided by the statistical uncertainty of the data-points [5].

6. $W\gamma\gamma$ and $Z\gamma\gamma$ production

Production of three-boson final states in proton-proton collisions is predicted by the $SU(2) \times U(1)$ gauge structure of the SM. Cross sections for these processes include contributions from quartic

Table 1: Expected and observed limits at 95% CL on single anomalous couplings (other couplings set to zero) [5]. First block corresponds to EFT parametrization, and second block to Vertex parametrization.

aTGC	expected limit	observed limit
$\frac{c_{WW}}{\Lambda^2}$ (TeV^{-2})	$[-8.73, 8.70]$	$[-9.46, 9.42]$
$\frac{c_W}{\Lambda^2}$ (TeV^{-2})	$[-11.7, 11.1]$	$[-12.6, 12.0]$
$\frac{c_B}{\Lambda^2}$ (TeV^{-2})	$[-54.9, 53.3]$	$[-56.1, 55.4]$
λ	$[-0.036, 0.036]$	$[-0.039, 0.039]$
Δg_1^Z	$[-0.066, 0.064]$	$[-0.067, 0.066]$
$\Delta \kappa_Z$	$[-0.038, 0.040]$	$[-0.040, 0.041]$

gauge couplings (QGCs), which are sensitive to new phenomena that modify those couplings. Simulated aQGC events are assigned a set of weights, each of which reproduces the effect of an anomalous QGC. The main background contribution in both analyses consists of events in which one or two jets are misidentified as photons. The background estimate is based on an analysis of the two-dimensional distribution of the charged hadron isolation variables $I_{ch,1}$ and $I_{ch,2}$ of the leading and subleading photon candidates, respectively. We measure fiducial cross sections of 4.9 ± 1.4 (stat.) ± 1.6 (syst.) ± 0.1 (lumi.) fb and 12.7 ± 1.4 (stat.) ± 1.8 (syst.) ± 0.3 (lumi.) fb for the $W\gamma\gamma$ and $Z\gamma\gamma$ processes, respectively. The measured cross sections are in agreement with the NLO theoretical predictions of 4.8 ± 0.5 fb and 13.0 ± 1.5 fb for the $W\gamma\gamma$ and $Z\gamma\gamma$ final states, respectively. These measurements correspond to significances for observing the signal of 2.6 and 5.9 standard deviations for the $W\gamma\gamma$ and $Z\gamma\gamma$ final states, respectively. Anomalous QGCs are modeled using a dimension-8 effective field theory parametrization [12]. Anomalous QGCs enhance the production of signal events at high momentum scales. The $W\gamma\gamma$ final state is used to place limits at 95% CL on anomalous quartic gauge couplings using a dimension-8 effective field theory. In particular, stringent limits are placed on the $f_{T,0}$ coupling parameter of $-33.5 < f_{T,0}/\Lambda^4 < 34.0 \text{ TeV}^{-4}$.

References

- [1] CMS Collaboration, JINST **3**, **S08004** (2008)
- [2] CMS Collaboration, Eur. Phys. J. **C 78** (2018) 165
- [3] CMS Collaboration, Phys. Lett. **B 766** (2017) 268
- [4] CMS Collaboration, CMS-PAS-SMP-16-006, [<https://cds.cern.ch/record/2160868>] 2016.
- [5] CMS Collaboration, CMS-PAS-SMP-16-012, [<https://cds.cern.ch/record/2209148>] 2016.
- [6] CMS Collaboration, JHEP **10** (2017) 072
- [7] M. Grazzini, et al. Phys. Lett. **B 761** (2016) 179
- [8] T. Gehrmann, et al. Phys Rev Lett. **113** 212001
- [9] J. Thaler, and K. Van Tilburg, JHEP **03** (2011) 015
- [10] S.D. Ellis, C.K. Vermilion, and J.R. Walsh, Phys. Rev. **D 81** (2010) 094023
- [11] K. Hagiwara, R. D. Peccei, D. Zeppenfeld, K. Hikasa, Nucl. Phys. **B 282** (1987) 253
- [12] C. Degrande, et al. Annals Phys. **335** (2013) 21